*Euro. Jnl of Applied Mathematics* (2017), *vol.* 28, *pp.* 716–735.  
doi:10.1017/S0956792516000498

# Determining the probability of correct resolution of the left–right ambiguity in towed array sonar

K. KAOURI[1] and D. J. ALLWRIGHT[2]

[1]*Department of Electrical Engineering, Computer Engineering and Informatics, Cyprus University of Technology, 30 Archbishop Kyprianou Str., Limassol 3036, Cyprus*
*email: katerina.kaouri@cut.ac.cy*
[2]*Smith Institute for Industrial Mathematics and System Engineering, Mathematical Institute, University of Oxford, Andrew Wiles Building, Radcliffe Observatory Quarter Woodstock Road, Oxford, OX2 6GG, UK*
*email: david.allwright@smithinst.co.uk*

(*Received 18 September 2015; revised 30 October 2016; accepted 02 November 2016; first published online 5 December 2016*)

When a towed sonar array is straight, it has the difficulty that it cannot distinguish a contact on the left from one at the same angle on the right. When the array is *not* straight and its shape known, we calculate the probability that the left–right ambiguity is resolved correctly, using the Neyman–Pearson hypothesis testing framework, assuming a delay-sum beamformer, a single-frequency contact, and Gaussian noise. We also initially consider the noise field to be uncorrelated and show that the evaluation of the probability of correct resolution reduces to evaluating a one-dimensional integral. We find, as expected, that the probability increases, as the signal-to-noise ratio and the lateral deviation of the array from straight increase. For demonstration purposes, we also evaluate the probability of correct resolution for two representative shapes the array might assume in practice. Finally, we consider a more realistic, correlated noise field and we show that the initial assumption of an uncorrelated noise field provides a good approximation when the lateral deviation of the array is sufficiently large.

**Key words:** 62F03 (Hypothesis testing), 62P30 (applications in engineering and mathematics), 94B70 (error probability), 74J05 (linear waves).

## 1 Introduction

Sound is the main means of exploration and communication in the sea [16], and detection and processing of sound signals plays a very important role in military and other applications, such as depth sounders, fish detection, and divers' equipment. The focus of this work is the mathematical treatment of left–right (LR) ambiguity in towed array sonar[1], a problem encountered in submarine acoustics [11, 16].

A towed array is a long, flexible hose (500–1,000 m) attached to the submarine (50–100 m) with a connecting cable (approximately 400 m). We consider a passive towed sonar[2] set that consists of a one-dimensional array of hydrophones (underwater microphones) that receive sound and a beamformer that processes the received sound—see Figure 1. The

[1] *Sonar* is an acronym for *so*und *na*vigation and *r*anging.
[2] A passive sonar only listens to incoming sounds in contrast to the active sonar that also sends out sound signals.

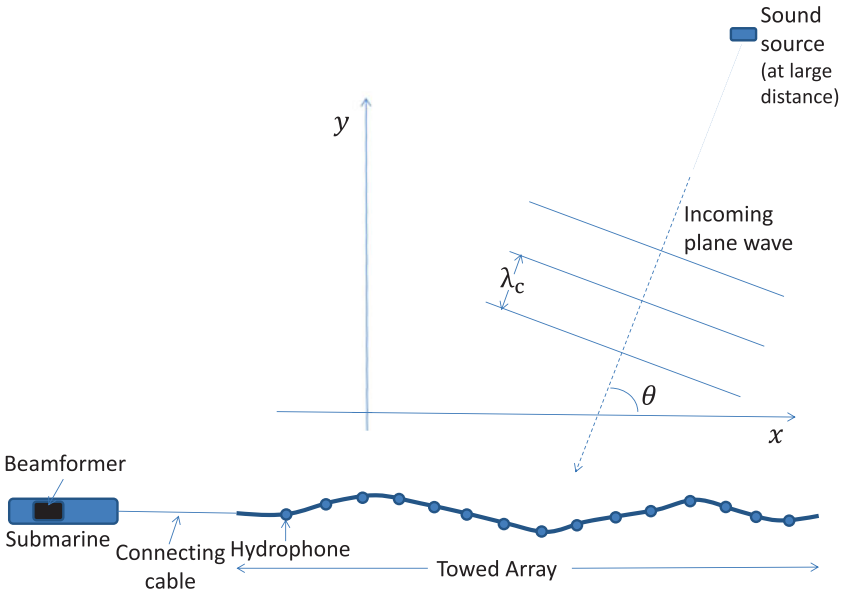


FIGURE 1. A towed array is attached to the submarine with a connecting cable. The towed array has hydrophones on it. We also show an incoming plane wave with wavelength $\lambda_c$, incident at an angle $\theta$ coming from a sound source that is far compared to the array length. We assume, as discussed, that the problem can be treated as two dimensional.

submarine, the towed array, and the sound source (the *contact*) are all submerged. When the array is straight, there is a complete axisymmetry about it and so it cannot distinguish sound sources on any circle about the array. For sources at a large distance compared to the array length, this means that there is ambiguity between the cone of the source directions making the same angle with the array axis. Since in practice a submarine is often aiming to detect sources whose depth is comparable to its own but whose range is much greater, this ambiguity shows up as an LR ambiguity. It is hence a good approximation to treat the problem as two dimensional, just considering the horizontal plane. (Figure 1 illustrates the two-dimensional problem.) When LR ambiguity exists the response of the beamformer is the same for the left and the right directions [11]. When the array is not straight and the shape is known, we will show in this work how to calculate the probability that the LR ambiguity is resolved correctly. Note that in this work we assume that the array shape has already been determined; in practice determining the array shape in the sea is a difficult task in itself and various methods of estimation have been presented in the literature—see, for example [13] and references therein.

Various methods have been proposed for resolving the LR ambiguity in underwater acoustics. For example, in [4], two or more line arrays are assumed towed at some separation, and both line arrays are beamformed together. Left and right cardioid responses are created by forming dipole and monopole virtual elements between the hydrophones of the two arrays. These cardioids are beamformed into left and right array responses, and targets correspond to enhanced response from the corresponding beamformer and suppressed response from the opposite beamformer. In [10], in the context of active sonar,

https://doi.org/10.1017/S0956792516000498 Published online by Cambridge University Press

the LR ambiguity is resolved through cardioid or triplet arrays that are towed arrays consisting of a line of triplets instead of a single line of hydrophones. Each triplet consists of three closely spaced omnidirectional hydrophones that are evenly mounted on a circle perpendicular to the array axis. The problem of resolving an LR ambiguity appears also in target tracking in astronomy, biomedical imaging, computer vision, etc. For example, in [9], LR ambiguity is resolved in the context of particle physics, and in particular in the use of HERA-B, a large-aperture high-rate spectrometer that studies collisions of protons with nuclei.

The paper is organised as follows. In Section 2, we first show how the LR ambiguity arises in the beamforming process in passive sonar. We then develop an appropriate hypothesis testing framework assuming an uncorrelated, Gaussian ambient noise field and obtain an expression for the probability of correct resolution (PCR) of the LR ambiguity, which can be conveniently cast as a one-dimensional integral, for any array shape. We subsequently study two model array shapes that mimic shapes the array might assume in practice. In Section 3, we consider the more realistic assumption of correlated noise and we modify our initial hypothesis testing framework, obtaining again the PCR as a one-dimensional integral, valid for any array shape. In Section 4, we summarise our conclusions and present further directions of work.

The methodology we use in this article has been developed in the M.Sc. dissertation of Kaouri [12] (University of Oxford); the second author was the supervisor of the dissertation[3].

## 2 Beamformer, signal, and noise models for an uncorrelated noise field

In this section, we are going to develop a model that will lead us to the evaluation of the PCR of the LR ambiguity. Therefore, we are going to first present our modelling assumptions.

- We treat the problem as two dimensional, which is a good approximation as discussed in Section 1. Therefore, we consider a two-dimensional array with the hydrophones at $\mathbf{x}_j = (x_j, y_j)$ and we consider incident plane waves $p(\mathbf{x}, t) = \Re(p_0 \exp(i(\omega t - \mathbf{k}.\mathbf{x})))$, where $\mathbf{k}$ is the incident wavevector $\mathbf{k} = k_0(\cos\theta, \sin\theta)$ and $k_0 = \omega/c$ is the acoustic wavenumber, where $c$, the sound speed, is assumed constant. We assume narrowband processing, so the acoustic wavenumber $k_0$ is fixed by the frequency of the sound source.
- The submarine has a delay-sum beamformer forming beams of the form

$$b(t) = \sum_{j=1}^{N_h} w_j p(\mathbf{x}_j, t - \Delta_j), \tag{2.1}$$

where $N_h$ is the total number of hydrophones, $w_j$ are the shading weights that play a role analogous to a windowing function in the Fourier transform [11, 16], and $\Delta_j$ are the delays that steer the beam in a particular direction.

[3] Note that [12] has been cited in subsequent work—see, for example, [2, 3, 5–7, 15].

https://doi.org/10.1017/S0956792516000498 Published online by Cambridge University Press

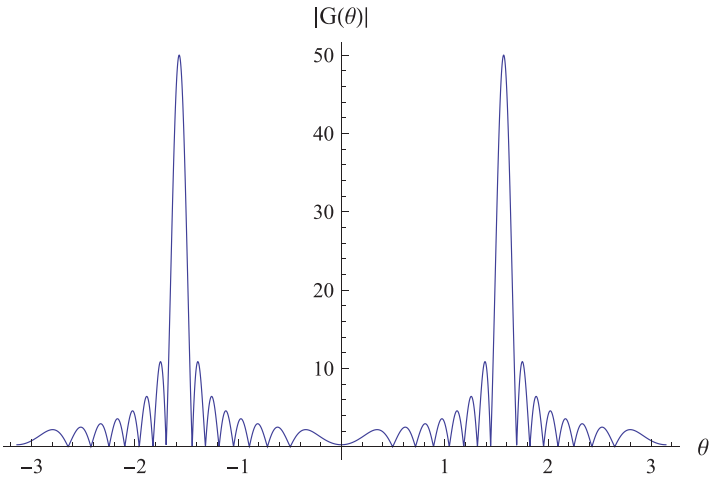


FIGURE 2. Visualisation of the left–right ambiguity when the array is straight; we see that the beamformer has equal response for $\theta = \pi/2$ and $\theta = -\pi/2$ due to the symmetry of $G(\theta)$. (We take $N_h = 50$, $\theta_b = \pi/2$, $k_0 = 1$, $w_j = 1$.)

- We assume that the array shape is known and that its shape has been determined using one of the methods developed for this purpose (see [13] and references therein).
- The noise field $n(\mathbf{x}, t)$ is assumed to be spatially and temporally uncorrelated and Gaussian with zero mean and variance $\sigma^2$.

In the beamforming process, we wish the array to have maximum response for incident waves from direction $\theta_b$, and then $\Delta_j = A + (x_j \cos\theta_b + y_j \sin\theta_b)/c$ for some constant $A$. The response of the beamformer to the incident plane wave is

$$b(t) = \Re\left(p_0 \exp(-i\omega A) \exp(i\omega t) G_b(\theta)\right), \tag{2.2}$$

where the beamformer gain, or directivity function, is

$$G_b(\theta) = \sum_{j=1}^{N_h} w_j \exp\left(ik_0(x_j(\cos\theta - \cos\theta_b) + y_j(\sin\theta - \sin\theta_b))\right). \tag{2.3}$$

If the shading weights $w_j$ are all positive, then clearly $|G_b(\theta)| \leqslant G_b(\theta_b) = \sum_j w_j$. However, if the array is straight, $y_j = 0$, and $G(\theta) = G(-\theta)$, dropping the subscript $b$ from now on. Therefore, the array has equally large response to waves incident from directions $\theta_b$ and $-\theta_b$. This is the ambiguity problem that arises for a straight array. In order to visualise the LR ambiguity in Figure 2, we plot $|G(\theta)|$ for $-\pi \leqslant \theta \leqslant \pi$ for a straight array and a wave incident at angle $\theta_b = \pi/2$. Note that in practice, the beam pattern is obtained by plotting the function $D(\theta) = 20\log_{10}(|G(\theta)|/\max_\theta|G(\theta)|)$, i.e., converting to decibels.

If the array is not straight, then $G(\theta)$ does not have this symmetry, and the beams formed with steer directions $\theta_b$ and $-\theta_b$ are different. Consequently, it is natural to attempt to resolve the LR ambiguity by reporting a contact on the right if the right beam has greater amplitude than the left, and vice versa.

https://doi.org/10.1017/S0956792516000498 Published online by Cambridge University Press

In this work, we assume that a sound source has already been detected by the submarine using some of the available methods, and that it is at a signal-to-noise ratio (SNR) large enough to resolve that its bearing is close to either $\theta_R$ on the right or $\theta_L = -\theta_R$ on the left. The positions of the peaks in the left and right responses will not be at exactly the angle of the source—that is the bearing-accuracy problem—but since our concern here is only with the ambiguity problem, not with bearing accuracy, we focus only on the question of distinguishing between $\pm\theta_R$. Our goal is to quantify the accuracy of the detection method by determining the probability of correctly resolving between the following two hypotheses.

**Null Hypothesis:** $H_0$:"Contact is on the Right".
**Alternative Hypothesis:** $H_1$:"Contact is on the Left".

Under the null hypothesis, the complex amplitudes from the right-pointing ($R$) and left-pointing ($L$) beams, in the presence of sea noise, will be, respectively,

$$X_R = a_0 G_R(\theta_R) + N_R, \quad X_L = a_0 G_L(\theta_R) + N_L, \tag{2.4}$$

where $G_R(\theta_R) = \sum_{j=1}^{N_h} w_j$, $G_L(\theta_R) = \sum_{j=1}^{N_h} w_j \exp(-2ik_0 y_j \sin\theta_R)$, and $a_0 = p_0 \exp(-i\omega A)\exp(i\omega t)$. The noise in the beams is denoted by $N$ and, since the sea noise is modelled as Gaussian, $N_L$ and $N_R$ are the complex Gaussian, with mean 0 and a circularly symmetric distribution characterized by the variance $V = \mathbb{E}(|N_i|^2) = \sigma^2$ where $i = R$ or $L$. When the array is not straight, we shall see in the discussion in Section 3 that $N_R$ and $N_L$ are approximately independent. Although this assumption is not always true, and for small lateral displacements of the array the correlation between the right and left lobes corresponding to the right and left beam is almost perfect, we are going to show that our analysis provides a good approximation in those parameter ranges for which there is sufficiently high PCR.

Under the alternative hypothesis, we form again the $L$ and $R$ beams, respectively $X_L$ with gain $G_L(\theta_L) = \sum_{j=1}^{N_h} w_j$, and $X_R$ with gain $G_R(\theta_L) = \sum_{j=1}^{N_h} w_j \exp(2ik_0 y_j \sin\theta_R)$, with everything else being the same as in the null hypothesis.

In practice, the $k$th component of the discrete Fourier transform (DFT) of the beams is taken [11]. We change the subscripts to 1 and 2 for right and left, respectively. Also, from now on we will call the frequency of interest $f$ for symbolic reasons. Therefore, the null hypothesis $H_0$ is recast as follows; for beam 1

$$b_1 = a + N_1,$$

where $a = (p_0 M/2)\exp(-i\omega A)\sum_{j=1}^{N_h} w_j$. We denote by $N_1$ the DFT of the noise component of beam 1; $N_1$ is a complex Gaussian random variable with zero mean and variance $\mathbb{E}(|N_1|^2) = \xi^2 = M\sigma^2$, where $M$ is the number of sampling times of the DFT [17]. For beam 2

$$b_2 = c_0 a + N_2,$$

with $c_0$ containing the information about the array shape. Since the noise is assumed spatially uncorrelated, it is isotropic, and since the only difference between $N_2$ and $N_1$ is

https://doi.org/10.1017/S0956792516000498 Published online by Cambridge University Press

that the beam is steered in a different direction, $N_2$ will have exactly the same probability distribution as $N_1$. For a general choice of shading weights $w_j$,

$$c_0 = \frac{G_2(\theta_1)}{G_1(\theta_1)} = \frac{\sum_j w_j \exp(-2ik_0 y_j \sin\theta_1)}{\sum_j w_j}. \tag{2.5}$$

Under the alternative hypothesis $H_1$, we have $b_1 = \bar{c_0}a + N_1$, $b_2 = a + N_2$.

The next step in the sound processing process in a passive sonar involves squaring the $k$th component of the DFT vector (square-law detector). The random variable $|b_1|^2$, arising through the square-law detector, has mean

$$\mathbb{E}(|b_1|^2) = |a|^2 + \xi^2, \tag{2.6}$$

and the SNR is given by $(\mathrm{SNR})_1 = |a|^2/\xi^2$ where $|a|^2 = |p_0|^2 M^2 \left(\sum_j w_j\right)^2$. (Note that the information about the phase $A$ is lost at this stage.) The random variable $|b_2|^2$ has mean

$$E(|b_2|^2) = |c_0|^2|a|^2 + \xi^2, \tag{2.7}$$

and the SNR now is given by $(\mathrm{SNR})_2 = |c_0|^2 a^2/\xi^2 = |c_0|^2(\mathrm{SNR})_1$. For the unshaded case, $w_j = 1$ and we have $c_0 = \frac{1}{N_h}\sum_j \exp\left(4\pi i f y_j/c\right)$ and therefore

$$|c_0|^2 = \frac{1}{N_h^2}\left(\left(\sum_j \cos(4\pi f y_j/c)\right)^2 + \left(\sum_j \sin(4\pi f y_j/c)\right)^2\right). \tag{2.8}$$

We notice that we have $|c_0| \leqslant 1$, as we expect under the null hypothesis; $|c_0|^2 = 1$ corresponds to $y_j = 0$, i.e., to a straight array. Under the alternative hypothesis $|b_1|^2$, $|b_2|^2$ switch the expressions they assume under the null hypothesis.

We are now going to scale the random variables $|b_1|^2$ and $|b_2|^2$ by defining $T_i = 2|b_i|^2/\xi^2$, where the subscript $i$ is 1 or 2. $T$ follows a standard non-central chi-squared distribution with two degrees of freedom and with non-centrality parameter $\lambda$, which we will denote by ${\chi'}^2_2(\lambda)$. (Note that we can easily prove this by evaluating the moment generating function of the variables $T_i$ and observing that it is the moment generating function of a non-central chi-squared distribution—detailed calculations can be found in [12], pp 20–21.) The probability density function (pdf) of $T \sim {\chi'}^2_2(\lambda)$ is given in [14]:

$$f(t|2,\lambda) = \exp(-(\lambda + t/2))I_0(\sqrt{\lambda t})/2, \tag{2.9}$$

where $I_0$ is the modified Bessel function of zero order. Therefore, our hypotheses $H_0$ and $H_1$ are recast as follows:

$$\begin{aligned} H_0 &: T_1 \sim {\chi'}^2_2(\lambda_1), \quad T_2 \sim {\chi'}^2_2(\lambda_2), \\ H_1 &: T_1 \sim {\chi'}^2_2(\lambda_2), \quad T_2 \sim {\chi'}^2_2(\lambda_1), \end{aligned}$$

where $\lambda_1 = |\mu|^2 = 2a^2/\xi^2 = 2(\mathrm{SNR})_1$, $\lambda_2 = |c_0|^2\lambda_1$. Under the approximation of treating $N_1$ and $N_2$ as independent, $T_1$ and $T_2$ are also independent random variables.

https://doi.org/10.1017/S0956792516000498 Published online by Cambridge University Press

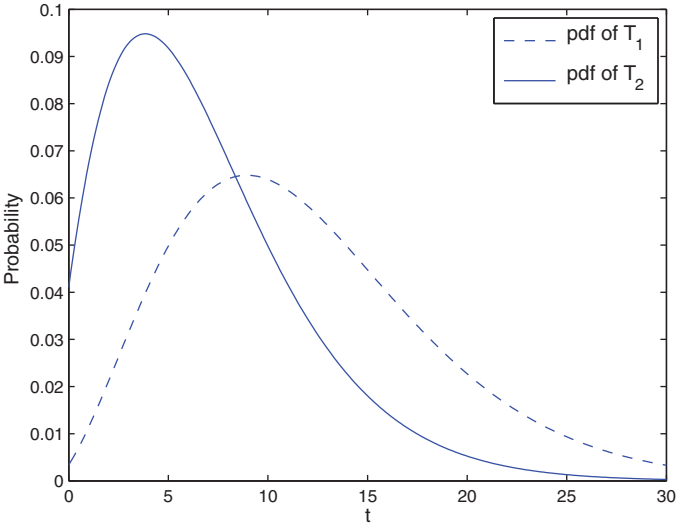


FIGURE 3. The pdfs of $T_1$ and $T_2$ under $H_0$ (SNR$=5$, $|c_0|^2 = 0.5$).

In Figure 3, we plot the pdfs of $T_1$ and $T_2$ under $H_0$. Under $H_1$, Figure 3 would look the same except that $T_1$ and $T_2$ would switch labels because of the symmetry of the hypothesis test.

### 2.1 The likelihood ratio rest

The likelihood ratio $L$ of the data vector $\mathbf{t} = (t_1, t_2)$ under the two hypotheses $H_0$ and $H_1$ is given in [17]:

$$L_{\mathbf{t}}(H_0, H_1) = \frac{f(t_1, t_2|H_1)}{f(t_1, t_2|H_0)} = \frac{f_1}{f_0}, \tag{2.10}$$

where $f_0$ and $f_1$ are, respectively, the joint pdfs of $T_1$ and $T_2$ under $H_0$ and $H_1$, where $\mathbf{t} = (t_1, t_2) = 2(|b_1|^2, |b_2|^2)/\xi^2$. Hence (2.10), using (2.9), reduces to

$$L = \frac{f(t_1|H_1)f(t_2|H_1)}{f(t_1|H_0)f(t_2|H_0)} = \frac{I_0(\sqrt{\lambda_2 t_1})I_0(\sqrt{\lambda_1 t_2})}{I_0(\sqrt{\lambda_1 t_1})I_0(\sqrt{\lambda_2 t_2})}. \tag{2.11}$$

According to the likelihood ratio test, we are going to reject $H_0$ if $L > l$, where $l$ is the critical value of the test. Consequently, $H_1$ will be rejected if $f_0/f_1 > 1/l$. Due to the symmetry between $H_0$ and $H_1$, we conclude that $l = 1$, and we reject the null hypothesis if $L > 1$. The size of the critical or rejection region is given by $P(L > 1)$, and $P(L < 1)$ is the $PCR$ and it is equal to the power of the test. Now, if we receive a louder signal in the left beam intuitively, we would deduce that the contact is on the left and we would reject the null hypothesis. Hence, we expect that we have $L > 1$ when $\lambda_2 < \lambda_1$ and $t_2 > t_1$. To

https://doi.org/10.1017/S0956792516000498 Published online by Cambridge University Press

prove this, we consider the difference of the numerator and the denominator of $L$:

$$D = I_0(\sqrt{\lambda_2 t_1})I_0(\sqrt{\lambda_1 t_2}) - I_0(\sqrt{\lambda_1 t_1})I_0(\sqrt{\lambda_2 t_2})$$
$$= \sum_{r=0}^{\infty} \sum_{0 \leqslant s < r} \lambda_1^s \lambda_2^s t_1^s t_2^s (\lambda_2^{(r-s)} - \lambda_1^{(r-s)})(t_1^{(r-s)} - t_2^{(r-s)}) C_{r,s}$$

using the power series for $I_0$ (see [1]), where $C_{r,s} = 1/(2^{2(r+s)} r!^2 s!^2)$. For $\lambda_2 < \lambda_1$ and $t_2 > t_1$, we have $D > 0$, and hence $L > 1$ as expected.

### 2.2 The probability of correct resolution

We have, thus, proved that with confidence quantified by $P(L < 1)$ we accept the hypothesis that the contact is on the right/left if the response is stronger on the right/left beam. We can write the PCR as the integral

$$P(L < 1) = \iint f_0(t_1, t_2) dt_1 dt_2,$$

where the region of integration is $t_1 \geqslant t_2$, as proved above. Since $f_0(t_1, t_2) = \mathrm{pdf}(t_1)\mathrm{pdf}(t_2)$, $P(L < 1)$ can be rewritten as the one-dimensional integral

$$P(L < 1) = \int_0^{\infty} \mathrm{pdf}(t_1)\mathrm{cdf}(t_1) dt_1, \tag{2.12}$$

where cdf stands for the cumulative density function and is given by

$$\mathrm{cdf}(t) = \int_0^t \mathrm{pdf}(\tilde{t}) d\tilde{t} = \int_0^t \frac{1}{2} e^{-\frac{\lambda+\tilde{t}}{2}} I_0(\sqrt{\lambda \tilde{t}}) d\tilde{t}. \tag{2.13}$$

Expression (2.12) is valid for any array shape. In Figure 4, we plot the PCR as a function of the two parameters SNR and $|c_0|^2$ (Matlab, conveniently, has the required pdf and cdf as built-in fuctions). We see that we have high PCR in the region of simultaneously high values of SNR and small values of $|c_0|^2$, which corresponds to large distortions of the array. As an example, we consider $|c_0|^2 \approx 0$; we see that PCR $\approx 0.9$ when SNR $\approx 3.2$. To achieve PCR $\approx 0.9$, for a larger value of $|c_0|^2 \approx 0.38$, a larger value of SNR, SNR $\approx 10$ is required. Also, when $|c_0|^2 \approx 1$, i.e., for an almost straight array, we confirm, that as expected, PCR $\approx$ 0.5 for all values of SNR, i.e., we have a 50–50 chance to resolve the ambiguity correctly.

Below we present some cross sections of Figure 4. In Figure 5, we fix SNR $= 10$ and vary $|c_0|^2$ from 0 to 1—we see that the PCR decreases as $|c_0|^2$ increases. In Figure 6, we fix $|c_0|^2 = 0.5$ and vary SNR. As SNR increases from 1 to 10, the PCR increases from approximately 0.59 to approximately 0.82 with a trend faster than linear.

### 2.3 Two model array shapes

In this section, we are going to analyse further the dependence of $|c_0|^2$ on the array shape by considering two model array shapes that are relevant in practice. When the array shape changes, we have a different dependence of $|c_0|^2$ on the parameter measuring the lateral displacement of the array from straightness.

https://doi.org/10.1017/S0956792516000498 Published online by Cambridge University Press

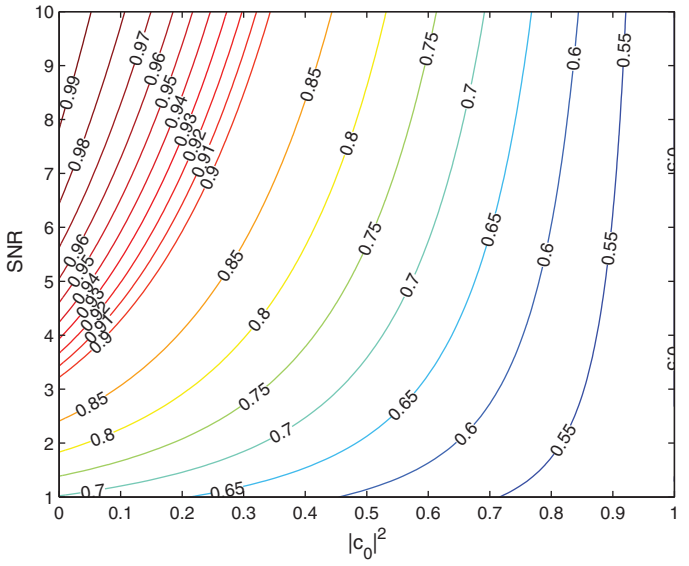


FIGURE 4. PCR as a function of $|c_0|^2$ and SNR.

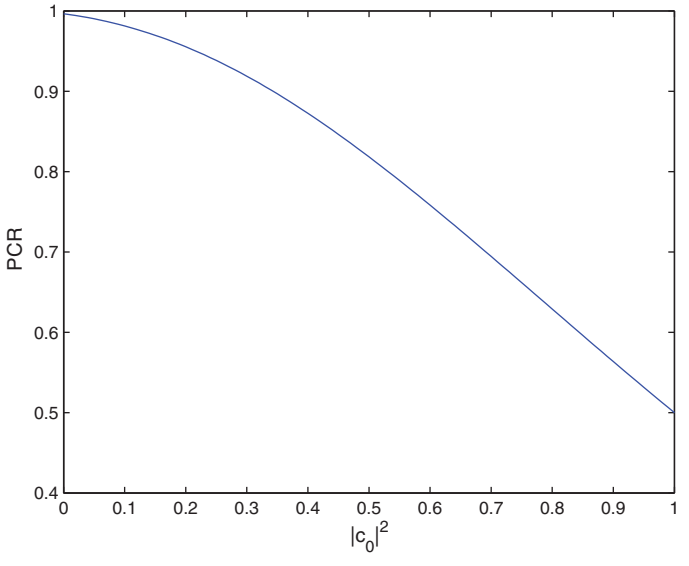


FIGURE 5. PCR as $|c_0|^2$ varies from 0 to 1, SNR = 10.

### 2.3.1 *First model array shape: sinusoid*

First, we model the array shape as one cycle of a sine wave, as might happen if the towing vessel undergoes oscillatory corrections to a steady course. We take the array shape

$$y = 2\alpha d \sin(2\pi x/L_0), \tag{2.14}$$

https://doi.org/10.1017/S0956792516000498 Published online by Cambridge University Press

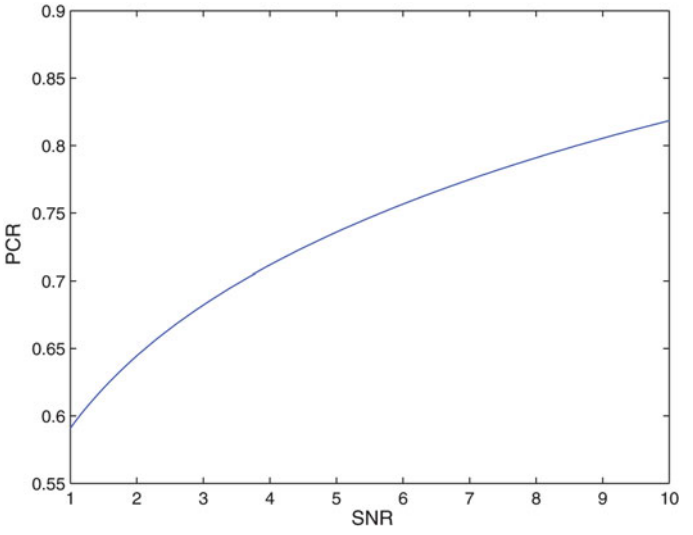


FIGURE 6. PCR for $|c_0|^2 = 0.5$ and SNR varying from 1 to 10.

where $d$ is the horizontal spacing between adjacent hydrophones and $L_0$ is the total length of the array, and $\alpha \geqslant 0$ is dimensionless and constant. Using $d = \lambda_c/2$, as most often in practice, the coordinates of the $j$th hydrophone are $x_j = jd$, $y_j = 2\alpha d \sin(2\pi x_j/L_0)$, i.e., we assume that the hydrophones are always equally spaced in the $x$-direction that is valid for small deviations of the array.

### 2.3.2 *Second model array shape: arc-of-a-circle*

As a second model array shape, we consider an arc of a circle with the angle subtended by the arc being $2\theta_s$. This is an appropriate model for the array shape when the towing vessel executes a turn of the appropriate radius. We consider the array at a time $t < \tau$ where $\tau$ is the characteristic timescale of the array dynamics and therefore the shape does not change. The length of the array is fixed, and the radius of the circular arc, $R_0$, satisfies $R_0 = L_0/(2\theta_s)$ that is as $\theta_s$ increases, the curvature of the arc increases. In this case, using plane polar geometry we can treat the hydrophones equispaced along the arclength $s$ instead of along the horizontal distance $x$, so $d$ is equal to $R_0\theta_0$ where $\theta_0 = 2\theta_s/(N_h - 1)$. The maximum angle subtended by the arc is $\pi$ so $0 \leqslant \theta_s \leqslant \frac{\pi}{2}$.

We see that the parameters $\alpha$ and $\theta_s$ for the first and second model array shapes, on which the size of the lateral displacement of the array depends respectively, enter the test through $|c_0|^2$ that appears in the non-centrality parameter $\lambda = |c_0|^2 |\mu|^2$. When the array tends to become straight, $\alpha$ and $\theta_s$ tend to zero, and $|c_0|$ tends to 1, the likelihood ratio tends to 1, and PCR tends to 0.5. In other words, the difference in the response of the left and right beam is decreasing, and it is therefore increasingly harder to resolve the LR ambiguity.

In Figure 7, we plot $|c_0|^2$ as a function of $W/\lambda_c$ where $W = 4\alpha d$ is the lateral displacement of the array, with no shading ($w_j = 1$). We take $N_h = 32$, $f = 100$ Hz, $c = 1,500$ m/s and $\theta_1 = \pi/2$. We observe that $|c_0|^2$ exhibits an oscillatory and decaying

https://doi.org/10.1017/S0956792516000498 Published online by Cambridge University Press

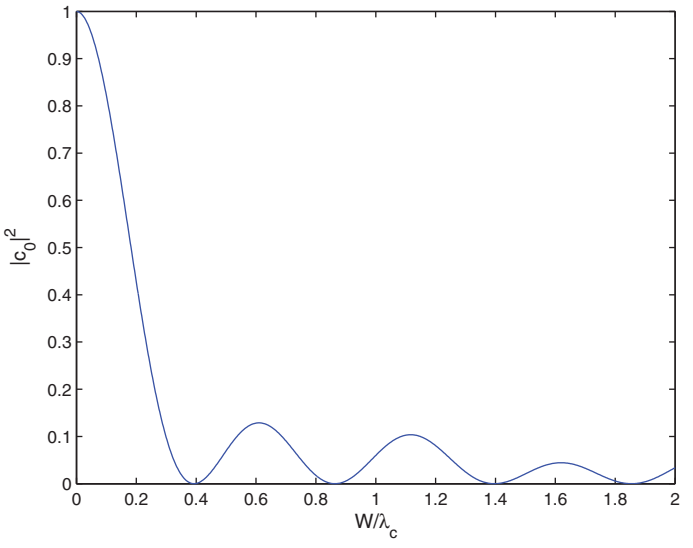


FIGURE 7. No shading; $|c_0|^2$ as a function of $W/\lambda_c$ (32 hydrophones, $c = 1,500$ m/s, $f = 100$ Hz, $\theta_1 = \pi/2$, $d = \lambda_c/2$).

behaviour as $W/\lambda_c$ is increasing. As $W/\lambda_c$ is increasing from 0 to approximately 0.25, $|c_0|^2$ decreases monotonically from 1 to approximately 0.12. For values of $|c_0|^2$ lower than 0.12, the graph is oscillatory and hence a particular value of $|c_0|^2$ may correspond to a set of increasing values of $W/\lambda_c$. However, when $0 \leqslant |c_0|^2 \leqslant 0.12$, for all possible values of $W/\lambda_c$, we can see in Figure 4 that we have a satisfactory probability of resolution since PCR $\geqslant 0.67$, for any value of SNR.

We further notice that $|c_0(\alpha)|^2 \approx J_0^2(4\pi\alpha)$ since

$$c_0 = \frac{1}{N_h}\sum_{j=1}^{N_h} \exp(4\pi i\alpha \sin(2\pi j/N_h)) \approx \frac{1}{2\pi}\int_0^{2\pi} \exp(4\pi i\alpha \sin\theta)d\theta = J_0(4\pi\alpha),$$

where $J_0$ is the Bessel function of zero order [1]. Exploring the latter approximation for $|c_0|^2$ and using that $J_0(x) = 0$ when $x = 2.4$, we find that for $\alpha = \frac{2.4}{4\pi} \approx 0.19$ we have $|c_0(\alpha)| = 0$. This corresponds to $\frac{W}{\lambda_c} = \frac{4\alpha d}{\lambda_c} = \frac{2.4}{\pi}\frac{d}{\lambda_c}$. The values of $W/\lambda_c$ that correspond to the zeros of $|c_0|$ give the best value of PCR out of all possible $W/\lambda_c$. Hence, for a given lateral displacement of the array, there are some frequencies at which we get best resolution.

In Figure 8, we plot $|c_0|^2$ as a function of $W/\lambda_c$ with the Dolph–Chebyshev shading, variants of which are used in practice to improve the beam shape and reduce sidelobes [16]. To implement the Dolph–Chebyshev shading, we use the Matlab command chebwin($N_h$, 50) that returns the $N_h$-point Chebyshev window with 50 dB of relative sidelobe attenuation. For illustration, a plot of the Chebyshev window is shown in Figure 9.

For the second model array shape, we plot $|c_0(\theta_s)|^2$ against $W/\lambda_c$, in Figure 10 for no shading, and in Figure 11 with the Dolph–Chebyshev shading, where we again take the Chebyshev window with 50 dB of relative sidelobe attenuation. In this case, the lateral

https://doi.org/10.1017/S0956792516000498 Published online by Cambridge University Press

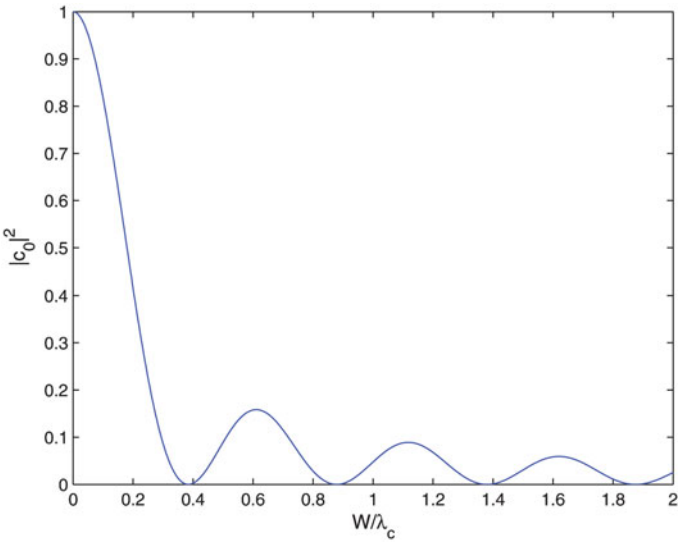


FIGURE 8. Dolph–Chebyshev shading; $|c_0|^2$ as a function of $W/\lambda_c$ (32 hydrophones, $c = 1,500$ m/s, $f = 100$ Hz, $\theta_1 = \pi/2$, $d = \lambda_c/2$).

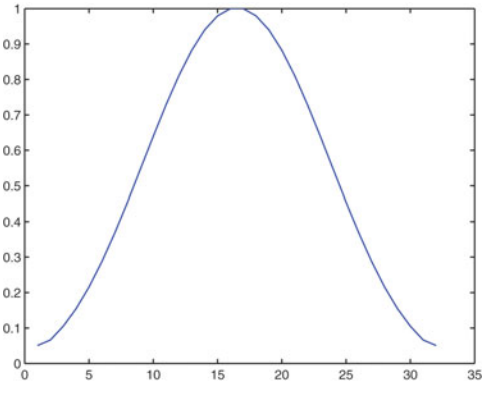


FIGURE 9. Chebyshev window for $N_h = 32$ and 50 dB of relative sidelobe attenuation.

displacement of the array is given by $W(\theta_s) = R(1 - \cos\theta_s)$. We take again $N_h = 32$, $f = 100$ Hz, $c = 1,500$ m/s, $\theta_1 = \pi/2$, and $d = \lambda_c/2$. (An approximate expression for $|c_0(\theta_s)|^2$ is not available in this case.) We see that for no shading when $W/\lambda_c = 1$ we have $|c_0|^2 \approx 0.28$ and with shading when $W/\lambda_c = 1$ we have $|c_0|^2 \approx 0.73$, which corresponds to a lower value of PCR. So although shading is introduced to improve the beam shape and reduce sidelobes, we see that it can also have adverse effects on the PCR. Taking the case of no shading, we observe that when the lateral deviation is of the order of $\lambda_c$ we already have a quite good resolution of the LR ambiguity since we can see from Figure 4 that when $|c_0|^2 = 0.28$, PCR$\geqslant 0.7$ for SNR$\geqslant 1.8$. In Figures 12 and 13, we again plot $|c_0|^2$ as a function of $W/\lambda_c$ for $N_h = 32$, $c = 1,500$ m/s, $f = 100$ Hz, and $\theta_1 = \pi/2$, but

https://doi.org/10.1017/S0956792516000498 Published online by Cambridge University Press

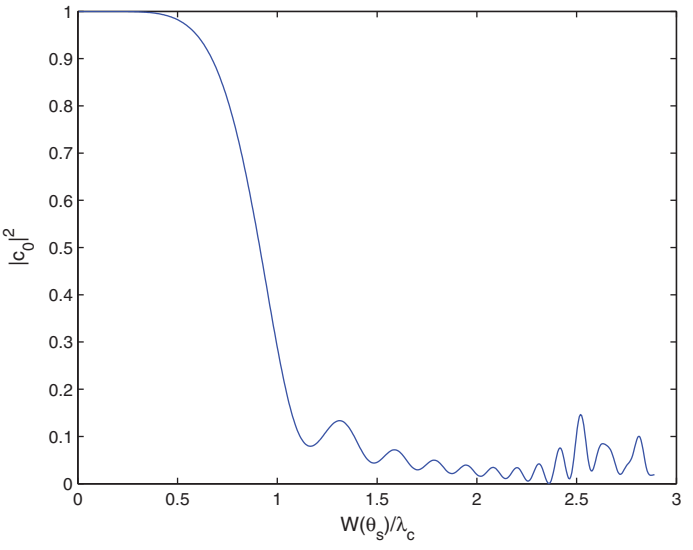


FIGURE 10. No shading; $|c_0|^2$ as a function of $W/\lambda_c$ (32 hydrophones, $c = 1,500$ m/s, $f = 100$ Hz, $\theta_1 = \pi/2$, $d = \lambda_c/2$).

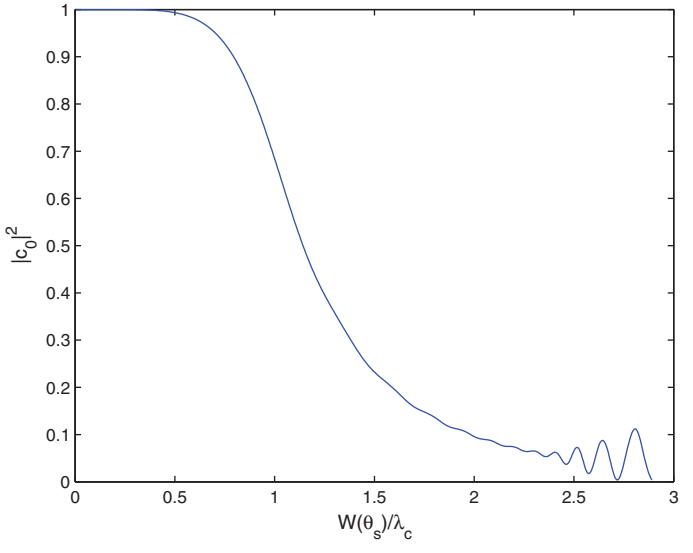


FIGURE 11. Dolph–Chebyshev shading; $|c_0|^2$ as a function of $W/\lambda_c$ (32 hydrophones, $c = 1,500$ m/s, $f = 100$ Hz, $\theta_1 = \pi/2$, $d = \lambda_c/2$).

$d = 0.4\lambda_c$. We see that for no shading when $W/\lambda_c = 1$ we have $|c_0|^2 \approx 0.1$ and with the Dolph–Chebyshev shading when $W/\lambda_c = 1$ we have $|c_0|^2 \approx 0.45$. Here, for the case of no shading, the resolution of the LR ambiguity is even more successful than when $d = \lambda_c/2$ since when $W$ is of the order of $\lambda_c$ that corresponds to $|c_0|^2 = 0.1$ we can see from Figure 4 that PCR$\geqslant 0.7$ for an even smaller value of SNR, SNR$\geqslant 1.3$.

https://doi.org/10.1017/S0956792516000498 Published online by Cambridge University Press

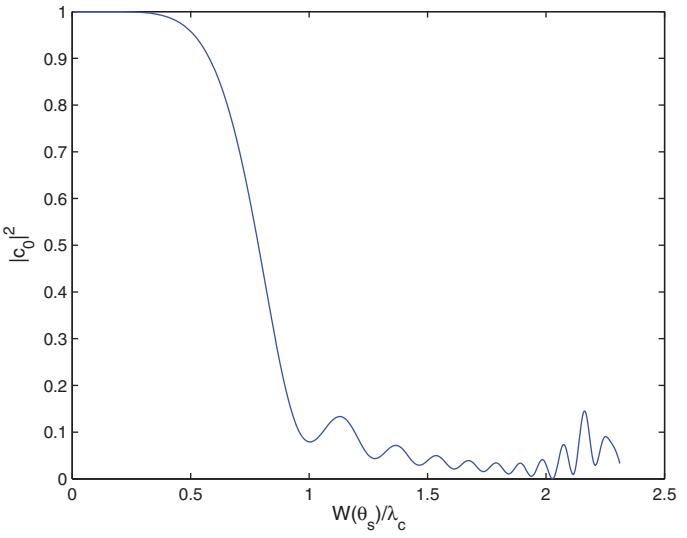


FIGURE 12. No shading; $|c_0|^2$ as a function of $W/\lambda_c$ (32 hydrophones, $c = 1,500$ m/s, $f = 100$ Hz, $\theta_R = \pi/2$, $d = 0.4\lambda_c$).

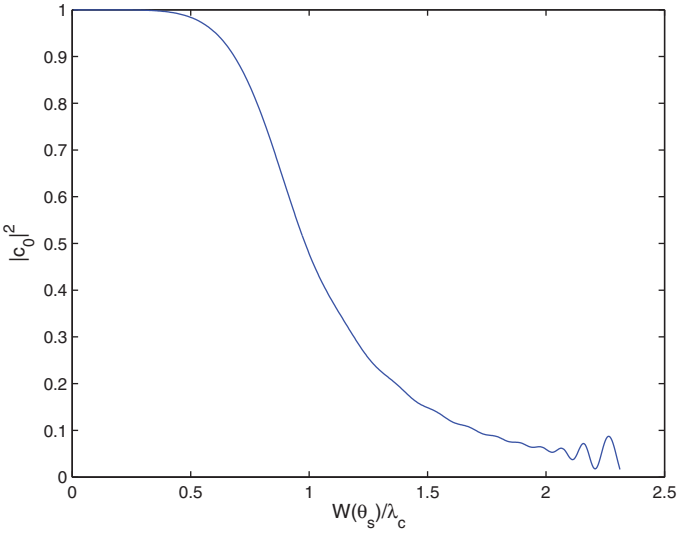


FIGURE 13. Dolph–Chebyshev shading; $|c_0|^2$ as a function of $W/\lambda_c$ (32 hydrophones, $c = 1,500$ m/s, $f = 100$ Hz, $\theta_R = \pi/2$, $d = 0.4\lambda_c$).

Up to now, we have assumed that the beams are uncorrelated for all values of $\alpha$ and $\theta_s$. However, when the array is almost straight $\alpha$ and $\theta_s$ are close to zero, and the beams are almost perfectly correlated. In Section 3, the beam correlation will be quantified appropriately and we will show that our uncorrelated-noise analysis indeed gives a good approximation to the PCR if $\alpha$ or $\theta_s$ are sufficiently large, which is often the case when resolving the LR ambiguity in practice.

https://doi.org/10.1017/S0956792516000498 Published online by Cambridge University Press

## 3 Resolution of the left-right ambiguity for a correlated noise field

We now drop the assumption that the noise field is spatially and temporally uncorrelated and we assume that the noise follows a stationary, homogeneous Gaussian process with zero mean and correlations given by

$$\mathbb{E}(n(\mathbf{x}_1, t_1)n(\mathbf{x}_2, t_2)) = \phi_n(\mathbf{x}_1 - \mathbf{x}_2, t_1 - t_2), \tag{3.1}$$

so $\phi_n$ is translationally invariant in space and time. Hence, the noise part of the right and left beams is given, respectively, by

$$b_1(t) = \sum_{j=1}^{N_h} n\left(\mathbf{x}_j, t - \Delta_j^{(1)}\right), \quad b_2(t) = \sum_{j=1}^{N_h} n\left(\mathbf{x}_j, t - \Delta_j^{(2)}\right).$$

Then, we calculate $\phi_{12}$, the correlation function between the two beams and using (3.1) we write

$$\phi_{12}(\tau) = \mathbb{E}(b_1(t)b_2(t-\tau)) = \sum_{m=1}^{N_h}\sum_{j=1}^{N_h} \phi_n(\mathbf{x}_j - \mathbf{x}_m, -\Delta_j^{(1)} + \Delta_m^{(2)} + \tau). \tag{3.2}$$

We take the DFT of beams $b_1$ and $b_2$ and denote their noise components by $N_1$ and $N_2$, respectively. The covariance of $N_1$ and $N_2$ is given by

$$\mathbb{E}(N_1\overline{N}_2) = \int G_1(\omega, \mathbf{u})\overline{G_2}(\omega, \mathbf{u})\Phi_{nn}(\omega, \mathbf{u})\, dA, \tag{3.3}$$

where $\mathbf{u}$ is a unit vector (ranging over the directions of incidence on the array), $G_1$ and $G_2$ are the beamformer gain functions for $b_1$ and $b_2$, and $dA$ is the element of area on the unit sphere of $\mathbf{u}$-vectors. The expectation of $|N_1|^2$ and $|N_2|^2$ will be given by similar expressions but with $|G_1|^2$ and $|G_2|^2$ in place of $G_1\overline{G_2}$. When $G_1$ and $G_2$ are separated enough that $\mathbb{E}(N_1\overline{N_2})$ is small compared with $\mathbb{E}(|N_1|^2)$ and $\mathbb{E}(|N_2^2|)$, $N_1$ and $N_2$ will be approximately independent and the analysis in Section 2 holds good. But for an array that is closer to being straight, $G_1$ and $G_2$ will be more similar, $\mathbb{E}(N_1\overline{N_2})$ will be larger, and one will need the analysis that follows. When $\Phi_{nn}(\omega, \mathbf{u})$ is isotropic, i.e., independent of the direction of $\mathbf{u}$, the correlation between the noise in the two beams is given by

$$\mathbb{E}(N_1\overline{N}_2) = \Phi_{nn}(\omega)4\pi \sum_{j,m} w_j w_m \exp(ik_0(\mathbf{b}_2.\mathbf{x}_m - \mathbf{b}_1.\mathbf{x}_j)\,\mathrm{sinc}(k_0|\mathbf{x}_j - \mathbf{x}_m|), \tag{3.4}$$

where $\mathbf{b}_1$ and $\mathbf{b}_2$ are the steer directions of the two beams.

The covariance matrix of the complex Gaussian vector $\mathbf{N}$ is now given by

$$V = \mathbb{E}(\mathbf{N}\mathbf{N}^\dagger) = \begin{pmatrix} \mathbb{E}(|N_1|^2) & \mathbb{E}(N_1\overline{N_2}) \\ \mathbb{E}(N_2\overline{N_1}) & \mathbb{E}(|N_2|^2) \end{pmatrix} = \begin{pmatrix} \xi^2 & \xi^2\beta \\ \xi^2\overline{\beta} & \xi^2 \end{pmatrix} \tag{3.5}$$

https://doi.org/10.1017/S0956792516000498 Published online by Cambridge University Press

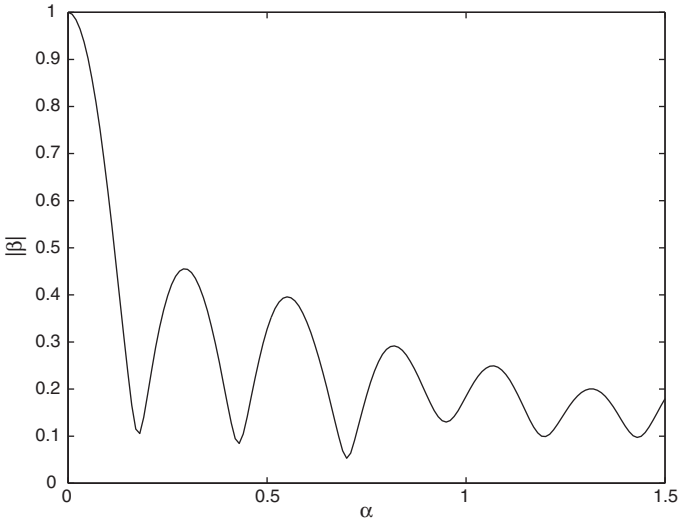


FIGURE 14. $|\beta|$ versus $\alpha$, $\alpha$ from 0 to 1.5.

which is no longer diagonal and $\beta = \mathbb{E}(N_1\overline{N}_2)/\mathbb{E}(|N_1|^2)$ quantifies the strength of the correlation between $N_1$ and $N_2$. Using (3.4), and assuming an unshaded array, we obtain

$$\beta = \frac{\sum_j \sum_m e^{-i\frac{\omega}{c}(y_j+y_m)}\text{sinc}\left(\frac{\omega}{c}\,|\mathbf{x}_m - \mathbf{x}_j|\right)}{\sum_j \sum_m e^{i\frac{\omega}{c}(y_j-y_m)}\text{sinc}\left(\frac{\omega}{c}\,|\mathbf{x}_m - \mathbf{x}_j|\right)}, \tag{3.6}$$

where $e^{i\frac{\omega}{c}(y_j-y_m)}$ and $e^{i\frac{\omega}{c}(y_j+y_m)}$ hold the information about the array shape.

For the two model array shapes considered earlier, we plot $|\beta|$ as a function of $\alpha$ in the range $[0, 1.5]$ in Figure 14 and $|\beta|$ as a function of $\theta_s$ in the range $[0, \pi/2]$ in Figure 15. For the first, sinusoidal, model shape $|\beta|$ decreases in an oscillatory manner, as $\alpha$ increases. We see that when $\alpha$ exceeds about 0.2, the value of $|\beta|$ is less than 0.5 so the correlation is not very strong and in this regime, the PCR obtained under the assumption of uncorrelated noise in Section 2 is a good approximation. For the second model array shape $|\beta|$ decreases in an oscillatory manner until approximately $\theta_s \approx \pi/3$, and for larger values of $\theta_s$ the peaks start increasing. Nevetheless, the uncorrelated-noise approximation is again valid for this model, since for the maximum angle $\theta_s = \pi/2$ the amplitude of the closest peak is still less than 0.5 as seen in Figure 15. Therefore, we can deduce that for both array shapes, the uncorrelated noise assumption leads to good estimates of the PCR when the lateral deviation of the array is sufficiently large.

To derive an expression for the PCR for any correlation coefficient $|\beta|$, we will again construct a hypothesis test with the same null and alternative hypotheses as in Section 2:

$$H_0 : b_1 = a + N_1, \quad b_2 = c_0 a + N_2$$
$$H_1 : b_1 = \bar{c_0} a + N_1, \quad b_2 = a + N_2,$$

where $a$ is in general complex due to an arbitrary phase added to it depending on how the signal is sampled and Fourier transformed. Scaling $b_1$, $b_2$ as in Section 2, we obtain the

https://doi.org/10.1017/S0956792516000498 Published online by Cambridge University Press

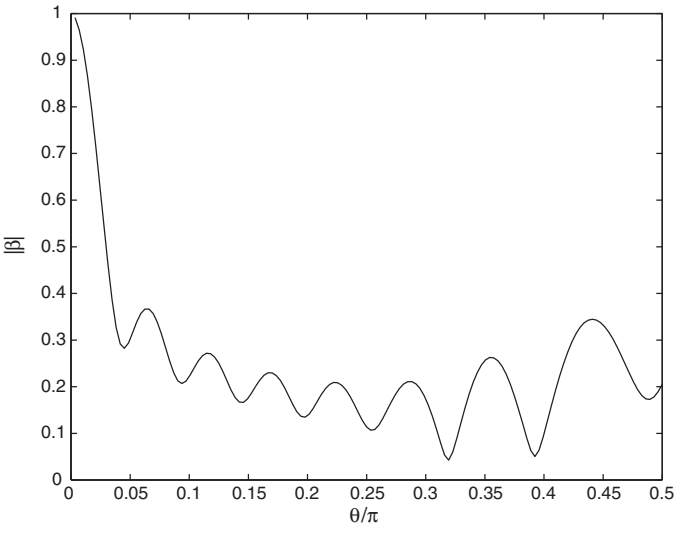


FIGURE 15. $|\beta|$ versus $\theta_s$, $\theta_s$ from 0 to $\pi/2$.

vector $\mathbf{z} = (z_1, z_2) = (\frac{\sqrt{2}}{\xi})(b_1, b_2)$ and $\mathbf{z}$ has a multivariate complex Gaussian distribution given in [8]:

$$f(z_1, z_2) = \frac{1}{\pi^2 \det V} \exp\left(-(\mathbf{z}-\mathbf{a})^\dagger V^{-1}(\mathbf{z}-\mathbf{a})\right) = \frac{1}{\pi^2 \xi^4 (1-|\beta|^2)} \times \exp\left(-\frac{1}{\xi^2(1-|\beta|^2)}\left(|z_1-a_1|^2 + |z_2-a_2|^2 - 2\Re(\beta(z_1-a_1)(\bar{z}_2-\bar{a}_2))\right)\right). \tag{3.7}$$

The generalised likelihood ratio is given by

$$L_G = \frac{\max_{\mathbf{a}} f(z_1, z_2, \mathbf{a}|H_1)}{\max_{\mathbf{a}} f(z_1, z_2, \mathbf{a}|H_0)} = \frac{\max_{\mathbf{a}}(f_1)}{\max_{\mathbf{a}}(f_0)},$$

where the vector $\mathbf{a}$ is unknown. We will obtain the optimum values of $\hat{a}_0$ and $\hat{a}_1$ that maximises $f_0$ and $f_1$, respectively. We find that

$$f_0 = \exp\left\{\frac{-|z_1-a|^2 - |z_2-c_0 a|^2 + 2\Re(\beta(\overline{z_1-a})(z_2-c_0 a))}{1-|\beta|^2}\right\}$$

is maximized by

$$\hat{a}_0 = \frac{z_1 + \bar{c}_0 z_1 - \bar{\beta}\bar{c}_0 z_1 - \bar{\beta} z_2}{1 + |c_0|^2 - 2\Re(\beta c_0)}$$

and, similarly, $f_1$ is maximised by

$$\hat{a}_1 = \frac{z_2 + c_0 z_1 - \beta c_0 z_2 - \bar{\beta} z_1}{1 + |c_0|^2 - 2\Re(\beta c)}.$$

https://doi.org/10.1017/S0956792516000498 Published online by Cambridge University Press

Using

$$z_1 - \hat{a}_0 = \frac{(\beta - \bar{c_0})(z_2 - c_0 z_1)}{1 + |c_0|^2 - 2\Re(\beta c)} \text{ and } z_2 - c_0\hat{a}_0 = \frac{(z_2 - c_0 z_1)(1 - \bar{\beta}\bar{c_0})}{1 + |c_0|^2 - 2\Re(\beta c_0)},$$

we find that

$$(f_0)_{\max} = k_0 \exp\left(\frac{-|z_2 - c_0 z_1|^2}{1 + |c_0|^2 - 2\Re(\beta c_0)}\right) \text{ and } (f_1)_{\max} = k_0 \exp\left(\frac{-|z_2 - \bar{c_0} z_1|^2}{1 + |c_0|^2 - 2\Re(\beta c_0)}\right).$$

According to the generalised likelihood ratio test, we are going to reject $H_0$ if $L_G > l$, where $l$ is the critical value of the test. Due to the symmetry of the test, the critical value will be $l = 1$ (as in the case of uncorrelated noise). Therefore, we accept $H_0$ if

$$(f_0)_{\max} > (f_1)_{\max} \Rightarrow |z_2 - c_0 z_1|^2 < |z_1 - \bar{c_0} z_2|^2. \tag{3.8}$$

We rearrange (3.8) as

$$|z_2|^2 - 2\Re(z_2\bar{c_0}\bar{z_1}) + |c_0|^2|z_1|^2 < |z_1|^2 - 2\Re(z_1 c_0 \bar{z_2}) + |c_0|^2|z_1|^2$$

$$\Rightarrow |z_2|^2(1 - |c_0|^2) < |z_1|^2(1 - |c_0|^2)$$

and since $|c_0|^2 < 1$ we accept $H_0$ when

$$|z_1|^2 > |z_2|^2 \Rightarrow t_1 > t_2. \tag{3.9}$$

This decision criterion is exactly the same as the decision criterion we derived for the uncorrelated noise field in Section 2, and therefore the intuitive decision procedure is still optimal. (So although it looked appealing in the beginning to use the additional available phase information, the calculation does not improve the test.) We again write the PCR as the integral

$$P(L_G < 1) = \iint f_0(t_1, t_2) dt_1 dt_2,$$

where the region of integration is $t_1 \geqslant t_2$, as given in (3.9). To derive the joint pdf of $T_1 = |z_1|^2$, $T_2 = |z_2|^2$, we substitute in $f_0$ the polar forms $z_1 = r_1 e^{i\theta_1}$, $z_2 = r_2 e^{i\theta_2}$, $\beta = |\beta| e^{i\phi_1}$, $c_0 = |c_0| e^{i\phi_2}$, where $r_1 = |z_1|$ and $r_2 = |z_2|$, and integrate $f_0(r_1, r_2, \theta_1, \theta_2)$ over $\theta_1$ and $\theta_2$, from 0 to $2\pi$. Evaluating the integral over $\theta_1$ first we obtain the one-dimensional integral

$$\int_0^{2\pi} \exp\left(-\frac{1}{\xi^2(1 - |\beta|^2)}(\cos(\theta_2 - \theta_1 + \phi_1) - 2ar_1 \cos\theta_1 + 2a|\beta||c_0|r_1 \cos(-\theta_1 + \phi_1 + \phi_2))\right)$$
$$\times I_0(\theta_2, \phi_1, \phi_2) d\theta_2, \tag{3.10}$$

which can be evaluated numerically. We have thus obtained an expression for the PCR as a one-dimensional integral. As discussed earlier, in cases where there is a useful PCR, the array distortion has to be large that corresponds to the correlation between the beams being small. Hence, the results for the *uncorrelated* case are a good approximation in those parameter ranges where there is useful probability of resolution.

https://doi.org/10.1017/S0956792516000498 Published online by Cambridge University Press

## 4 Conclusions and discussion

The resolution of the left–right ambiguity problem for a towed array sonar set has been considered theoretically. The successful resolution of the ambiguity always depends on using the fact that the array is not straight and depends on having some independent estimate of the array shape, such as that provided by heading sensors on the array. We have assumed a simple scenario where a single frequency contact has been detected and has been located in direction *apart from* the question of resolving the left–right ambiguity. Intuitively, the most natural way of resolving the ambiguity is to form left-pointing and right-pointing beams and decide that the contact is on the left or right according to which beam detects the greater amplitude.

We have analysed this problem mathematically and find that it is considerably simplified if it is assumed that there is no correlation between the noise in the left and right beams. In that case, the intuitive procedure has been shown to be justified by the likelihood ratio test, and the probability of correct resolution of the ambiguity has been calculated. It depends on the SNR of the contact, and it also depends on how much the array deviates from a straight line. If the acoustic wavelength is $\lambda_c$, we considered the case where the array shape is sinusoidal with lateral displacement $W = 4\alpha d$, and calculated the probability of correct resolution of the ambiguity. We showed, for instance, that in order to have 80% probability of correct resolution, the value of $W$ when $d = \lambda_c/2$ must be at least $2\lambda_c$, i.e., the array deviates from straight by $\pm\lambda_c$ on each side.

We further considered the problem when *correlation* between the noise in the two beams is taken into account. We have shown that even in this case the intuitive decision procedure is still optimal, and we have again obtained an expression for the probability of correct resolution as a one-dimensional integral. In fact, in cases where there is a useful probability of resolution, the lateral deviation parameter $\alpha$ has to be large, and this in itself causes the correlation between the beams to be small. Hence, the results for the *uncorrelated* case should be a good approximation in those parameter ranges where there is good probability of resolution.

## Acknowledgement

This work was supported by a STSM Grant from COST Action TD1409 (Mathematics for Industry Network).

## References

[1] Abramowitz, M. & Stegun, I. A. (1972) *Handbook of Mathematical Functions*. Wiley, New York.

[2] Bin, Z. (2010) Effects of sonar shape distortion on time delay estimation method for left/right discrimination. In: *2nd International Conference on Multimedia and Information Technology (MMIT)*, Vol. 2, IEEE, pp. 78–81.

[3] Bousnina, I., Stéphenne, A., Affes, S. & Samet, A. (2011) A new low-complexity angular spread estimator in the presence of line-of-sight with angular distribution selection. *EURASIP J. Adv. Signal Process.* **2011**(1), 1–16.

[4] Danforth, C. W. (2000) Acoustic applications of phased array technology. Acoust. Bull. **25**(6), 9–15.
[5] Dang, V., Lee, Y. & Lee, S. (2011) Characterizing a moving source in wireless sensor networks from the view of maximum likelihood. In: *2nd International Conference on Next Generation Information Technology (ICNIT)*, IEEE, pp. 18–22.
[6] Dang, V., Phan, T., Le, B., Lee, Y. & Lee, S. (2011) Clustering based multi-object positioning system. In: *International Conference on Advanced Technologies for Communications (ATC)*, IEEE, pp. 40–44.
[7] Dang, V. (2012) *Multiple Object Localization based on Acoustic Signals in Wireless Sensor Networks*. PhD thesis, Kyung Hee University, Korea.
[8] Goodman, N. R. (1963) Statistical analysis based on a certain multivariate complex Gaussian distribution (An introduction). *Ann. Math. Stat.* **34**(1), 152–177.
[9] Gorbunov, Y. (2003) *Pattern Recognition in the Inner Tracking System of HERA-B and Measurement of the V0 Production Cross Section in pN Collisions*. PhD thesis, Siegen University, Germany, 2003.
[10] Haralambus, G. & Bardacci, A. (2006) *Unambiguous Triplet Array Beamforming and Calibration Algorithms to Facilitate an Environmentally Adaptive Active Sonar Concept*. Technical report, NATO Undersea Research Centre, Italy.
[11] Hodges, R. P. (2011) *Underwater Acoustics: Analysis, Design and Performance of Sonar*, John Wiley and Sons, New York, USA.
[12] Kaouri, K. (2000) *Left-Right Ambiguity Resolution in Towed Array Sonar*. Master's thesis, University of Oxford, UK.
[13] Odom, J. L. & Krolik, J. (2013) Heading and hydrophone data fusion for towed array shape estimation. In: *Proceedings of Meetings on Acoustics*, Vol. 19, Acoustical Society of America, p. 055081.
[14] Rice, A. C. (1995) *Mathematical Statistics and Data Analysis*, Duxbury Press, California, USA.
[15] Stiles, Z. H. (2013) *Dynamic Towed Array Models and State Estimation for Underwater Target Tracking*, PhD thesis, Naval Postgraduate School, Monterey, CA USA.
[16] Urick, R. J. (1975) *Principles of Underwater Sound*, McGraw-Hill, New York, USA.
[17] Van Trees, H. L. (1968) *Detection, Estimation and Modulation Theory-Part I*, John Wiley and Sons, New York.